Biosensors and Bioelectronics 87 (2017) 101–107

Contents lists available at ScienceDirect

Biosensors and Bioelectronics

journal homepage: www.elsevier.com/locate/bios

Horseradish peroxidase supported on porous graphene as a novel sensing platform for detection of hydrogen peroxide in living cells sensitively

Yidan Liu, Xiuhui Liu *, Zhipan Guo, Zhongai Hu, Zhonghua Xue, Xiaoquan Lu *

Key Laboratory of Bioelectrochemistry & Environmental Analysis of Gansu Province, College of Chemistry & Chemical Engineering, Northwest Normal University, Lanzhou 730070, China

ARTICLE INFO

Article history:
Received 10 June 2016
Received in revised form
23 July 2016
Accepted 5 August 2016
Available online 5 August 2016

Keywords:
Porous graphene
Horseradish peroxidase
Electrochemical biosensor
Hydrogen peroxide detection
Cell tracking

ABSTRACT

A viable and simple method for preparing porous graphene network using silver nanoparticles (AgNPs) etching was proposed, and a sensitive biosensor was constructed based on the porous graphene (PGN) and horseradish peroxidase (HRP) to measure the release of H_2O_2 from living cells. Owing to the large surface area and versatile porous structure, the use of nanoporous materials can significantly improve the analysis performance of the biosensor by loading large amounts of enzyme and accelerating diffusion rate. Meanwhile, the constructed electrode exhibited excellent electrochemical performance toward H_2O_2 with a determination limit as low as 0.0267 nM and wide linear range of 7 orders of magnitude, which was superior to other H_2O_2 electrochemical sensors. Thus, this novel biosensor can detect the H_2O_2 release from living cells not only under normal physiological conditions (10^{-8}–10^{-7} M) but also in emergency state with the increased concentration ($\sim 10^{-4}$ M). This work provides tremendous potential for real-time tracking of the secretion of H_2O_2 in different types of physiological and pathological investigations.

© 2016 Elsevier B.V. All rights reserved.

1. Introduction

Reactive oxygen species (ROS) are important intracellular signaling molecules, mainly regulating protein synthesis, DNA damage, cell apoptosis, etc. (Chang et al., 2013). Nevertheless, the excessive amount of ROS accumulation in cells could lead to a series of cell damage and cause aging and disease, including cardiovascular disease, Alzheimer's disease and cancer (Pagliari et al., 2012; Wu et al., 2011). H_2O_2, a common representative of reactive oxygen species (ROS), has received much consideration since its long lifetime allows it to penetrate into other cellular compartment to induce various harmful biological modifications potentially. It is closely related to people's safety and health (Zhang et al., 2013; Trachootham et al., 2009). Hence, developing a rapid, sensitive, and accurate method to measure H_2O_2 dynamic release process from living cells is essential in studying the biological effect of H_2O_2 and preventing relative diseases associated with human inflammatory (Rhee et al., 2010; Zhang et al., 2014a; Maji et al., 2014; Oh et al., 2012).

Compared with fluorometry, spectrophotometry, and chromatography, electrochemical methods are more effective for in situ and real-time analysis of H_2O_2 due to their fast response, good selectivity, high sensitivity, excellent reproducibility, and facile operation (Yuan et al., 2012; Xu et al., 2014; Xi et al., 2015). In particular, electrochemical methods based on the catalytic reduction of H_2O_2 by the natural enzyme, for example, horseradish peroxidase (HRP), have witnessed an increasing interest because of their high efficiency, good selectivity and sensitivity toward H_2O_2 (Chen et al., 2016; Feyzizarnagh et al., 2016). However, the immobilization and stabilization protocol of the enzyme on the electrode are complicated, and the activity of the enzyme electrode is easy to reduce (Lippert et al., 2011). Moreover, due to the low concentration of H_2O_2 in cell, the detection limit still needs to be improved. In order to solve these problems, it is necessary to develop the excellent support matrix that provide better environment for loading the enzyme efficiently and maintaining the enzymatic bioactivity.

Porous graphene, the isolated two-dimensional carbon nanomaterial with some holes/pores within the atomic plane, has attracted great attention recently in the fields of nanomaterial and electrochemistry on account of its extraordinary physiochemical properties including larger surface area, higher electron conductivity and better biocompatibility (Zhou et al., 2014; Xi et al.,

* Corresponding authors.
E-mail addresses: liuxh@nwnu.edu.cn (X. Liu), luxq@nwnu.edu.cn (X. Lu).

http://dx.doi.org/10.1016/j.bios.2016.08.015
0956-5663/© 2016 Elsevier B.V. All rights reserved.

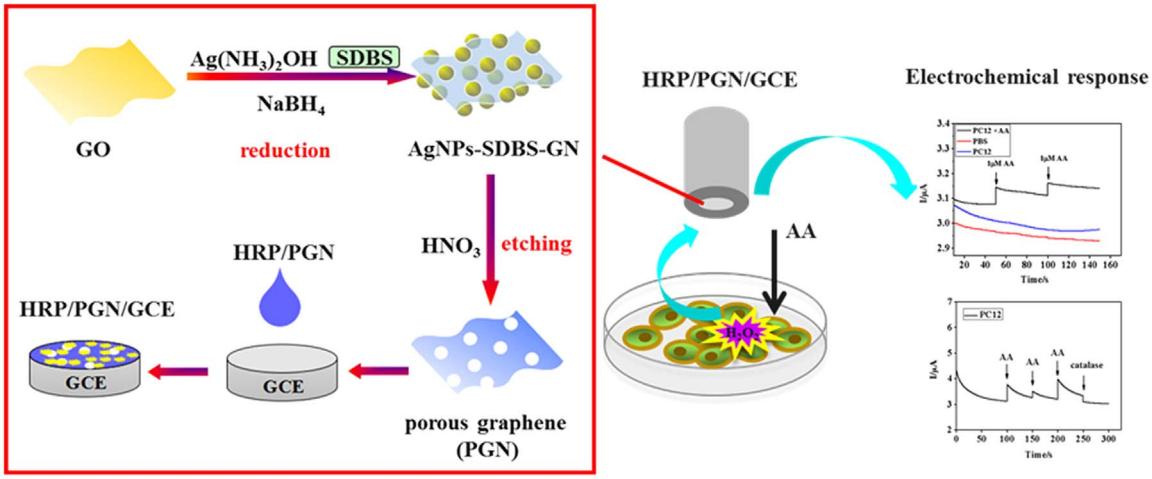

Scheme 1. Schematic of the HRP/PGN modified GCE used for detecting H_2O_2 release from cells stimulated with ascorbic acid (AA).

2012). Moreover, construction of graphene into porous structure can effectively prevent aggregation of graphene sheets (Han et al., 2014; Jiang and Fan, 2014), and is beneficial of the adsorption of enzyme. Meanwhile, nanopores are advantageous for ions passing through (Sint et al., 2008). These merits made porous graphene (PGN) an excellent supporting material. However, little work is available on the application of enzyme/porous graphene as electrochemical sensors.

In this work, we developed a novel enzymatic H_2O_2 sensor based on PGN and HRP to measure the release of H_2O_2 from living cells (Scheme 1). As demonstrated later, such a biosensor can facilitate the electron transfer of HRP and improve analytical performance for the determination of H_2O_2. Most importantly, the outstanding features of PGN, combined with the excellent selective catalysis of HRP, enable this biosensor to be used for determining the release of H_2O_2 from living cells with satisfaction.

2. Material and methods

2.1. Apparatus

The transmission electron microscopy (TEM) images were obtained from JEM-3010 transmission electron microscope (JEOL Co., Ltd., Japan). Raman spectra were recorded on a Renishaw inVia Raman microscope system with 632.8 nm laser excitation. Nitrogen sorption isotherms were obtained with a Micromeritics TriStar II 3020 surface area and porosity analyser at 77 K. The samples were degassed overnight at 110 °C. The Brunauer–Emmett–Teller (BET) method was used to calculate the specific surface area. Electrochemical measurements were performed on a CHI660C electrochemical workstation (Austin, TX, USA) using a three-electrode system with a glassy carbon electrode (GCE, d = 3.0 mm) or modified GCE as the working electrode, a saturated calomel electrode (SCE) and a platinum electrode as the reference and counter electrode, respectively. All potentials given in this paper were referred to the SCE. Before each electrochemical measurement, solutions were thoroughly deoxygenated by bubbling nitrogen through the solution for at least 20 min to remove dissolved oxygen.

2.2. Reagents

Graphite (99.99% SP-1, Bay carbon) with average particle size of 45 μm was obtained from Shanghai Chemical Reagent (Shanghai, China). Hydrogen peroxide solution (30 wt%) and nitric acid (HNO_3) were purchased from Beijing Chemical Reagent (Beijing, China). Silver nitrate ($AgNO_3$) and ammonia ($NH_3 \cdot H_2O$) were bought from Xi'an Chemical Reagent (Xi'an, China). Sodium dodecyl benzene sulfonate (SDBS) and sodium borohydride ($NaBH_4$) were obtained from Tianjin Chemical Reagent (Tianjin, China). Horseradish peroxidase (HRP) and ascorbic acid (AA) were obtained from Sigma. The catalases (2000–4000 units/mL) was purchased from Beijing Chemical Reagent (Beijing, China). A 0.2 M phosphate buffer solution (PBS, pH 7.0) comprising NaH_2PO_4 and Na_2HPO_4 was used as the supporting electrolyte. A physiological PBS solution containing KH_2PO_4 (1.76 mM), Na_2HPO_4 (10.14 mM), NaCl (136.75 mM), and KCl (2.28 mM), was mainly used for washing of PC12 cells and observing the release of H_2O_2 from the cells. Other chemicals were all of analytical grade, and the solutions were prepared by doubly distilled water.

2.3. Preparation of the porous graphene

Graphene oxide (GO) dispersions were prepared from the graphite powder by a modified Hummers' method (Li et al., 2008). The AgNPs-graphene nanocomposites were carried out by a facile and versatile hydrothermal synthetic strategy and the detailed preparation steps are as follows: as-prepared graphene oxide (0.05 g) was initially dispersed into 50 mL water under ultrasonic for 3 h, and SDBS (0.05 g) was dissolved into 20 mL water. Then SDBS solution was added into aqueous GO dispersion followed by approximately 60 min of ultrasonication to achieve the SDBS-GO suspension. $NH_3 \cdot H_2O$ (3%) was dropped into aqueous $AgNO_3$ solution (0.02 M, 10 mL) continuously until the precipitates disappeared and the Tollens' reagent was obtained. Next, the Tollens' reagent was dropped into as-synthesized SDBS-GO suspension and adequately stirred for 3 h. Following this, 70 mL of $NaBH_4$ (40 mM) solution was added into the above mixture at a stirring rate of 600 rpm for 12 h at 90 °C. The solution was filtered by nylon membrane with 0.22 μm pores, thoroughly washed with water to remove the free materials in the solution. The obtained black product, named as AgNPs-graphene (AgNPs-GN), was immersed in aqueous HNO_3 solution (1.0 M) and stirred for 3 days to remove AgNPs. Finally, the porous graphene (PGN) sample was collected by filtration and washed with water and ethanol. The product was obtained through freeze drying process.

2.4. Preparation of the H_2O_2 sensor

Prior to the modification, the glassy carbon electrode (GCE) was polished with 1.0, 0.3 and 0.05 μm alumina slurry to a mirror-like,

respectively, followed by rinsing thoroughly with doubly distilled water. 8 μL of PGN aqueous solution (1.0 mg mL^{-1}) was dropped on the surface of a GCE and dried in air to obtain PGN/GCE-1 and then this modified electrode was soaked in HRP aqueous solution (5.0 mg mL^{-1}) for 1 h to gain HRP/PGN/GCE-1. In addition, in order to detect H_2O_2 more sensitive, we have adopted another approach to construct the modified electrode based on the porous graphene. The HRP@PGN solution was initially prepared by mixing 5 mg horseradish peroxidase (HRP) with 2 mL porous graphene solution (0.5 mg mL^{-1}) under ultrasonication for 10 min at room temperature. Then 6 μL of the HRP@PGN solution was dropped on the surface of a GCE and dried in air, and was denoted as HRP/PGN/GCE-2. Graphene nanosheet (GN) could also be used to prepare modified electrode with the same condition mentioned above, and the relative sample was named as HRP/GN/GCE-2.

2.5. Cell culture

PC12 (rat adrenal medulla pheochromocytoma) cells were obtained from Institute of Hematology, Chinese Academy of Medical Sciences. They were maintained in DMEM (high glucose, Gibco) medium supplemented with 10% heat-inactivated fetal calf serum (Sigma, USA), 100 U/mL penicillin (Sigma, USA), and 100 mg/mL streptomycin (Sigma, USA) at 37 °C with 5% CO_2 in a 95% humidified atmosphere.

2.6. Electrochemical detection of H_2O_2 released from cells

PC12 cells grown in 25 cm^2 cell culture flasks were seeded in a 6-well plate (1.0×10^5 cells per well) for 24 h for electrochemical experiments. Cell number was estimated by a cell counter. The media was removed and the cells were washed two times with deoxygenated phosphate-buffered saline, and then 3 mL deoxygenated phosphate-buffered saline was added for real sample measurements. The amperometric detection of the release flux of H_2O_2 from PC12 cells was performed using the HRP/PGN/GCE-2 at −0.7 V (vs SCE), which was placed inside the 6-well plate and exposed to the cell solution. Ascorbic acid (AA) was injected to the cells suspension, which can motivate cells generation of H_2O_2 and H_2O_2 produced from the cancer cell was monitored by amperometric measurements. As a control group, 300 μL of catalase (2000–4000 units/mL) was then added to the solution that contained cells.

3. Results and discussion

3.1. Characterization of the porous graphene

3.1.1. Morphological and structural characterization

We have initially characterized the porous graphene (PGN) using transmission electron microscopy (TEM), Raman spectra and Nitrogen adsorption/desorption isotherm.

The porous graphene was prepared using silver nanoparticles (AgNPs) to etch graphene sheets by a one-pot reduction method. From the TEM images of Fig. 1A, one can see that spherical silver particles with diameters of 10–30 nm were embedded in the graphene film, and the corresponding energy dispersive X-ray spectroscopy (EDX) was shown in inset of Fig. 1A, displaying strong peaks of C, O and Ag. Furthermore, as shown in Fig. 1B, the high-resolution TEM (HRTEM) image of AgNPs–GN nanocomposites reveals that AgNPs with a highly ordered crystalline structure displays a lattice spacing of 0.236 nm, corresponding to the Ag (111) plane (Qin et al., 2012). When AgNPs were removed by treatment with HNO_3, well-developed nano-scaled porous structure can be observed in the graphene surface, and marked by the red circles in Fig. 1C, which are better than our previous work (Liu et al., 2015b). The corresponding EDX was also shown in inset of Fig. 1C, and there are only peaks of C and O, suggesting an effective removal of AgNPs in the graphene by acid. As a comparison, Fig. 1D is TEM of the graphene (GN) sample, which was prepared without AgNPs etching, revealing a view of graphene nanosheets clearly.

Another evidence for the introduction of pores on graphene sheets is the change of the D/G intensity ratio in Raman spectrum. Fig. 1E shows the Raman spectrum of GO and PGN. Compared with GO ($I_D/I_G=0.9$), there is a high D/G intensity ratio for PGN ($I_D/I_G=1.3$), suggesting more defects on the graphene sheets (Fan et al., 2012; Cao et al., 2015).

Moreover, the N_2 adsorption/desorption plots of PGN sample (Fig. 1F) show a type II isotherm with a steep increase of nitrogen absorption at a high relative pressure and the hysteresis loop of adsorption/desorption isothermal, indicating that the main pores are contributed by mesoporous (Fu et al., 2006). The BET specific surface area and pore volume of PGN are 430.27 $m^2 g^{-1}$ and 0.44 $cm^3 g^{-1}$, which are higher than pure graphene (79.05 $m^2 g^{-1}$ and 0.14 $cm^3 g^{-1}$) (Liu et al., 2015a). The pore size distribution of PGN is exhibited in the inset of Fig. 1F, illustrating that the pore sizes are mainly distributed at 20 nm, which is in agreement with the TEM image of Fig. 1C.

3.1.2. Electrochemical characterization of PGN/GCE

In order to verify the electrical conductivity of prepared composites, a comparative study of the cyclic voltammetry for the different modified electrodes was carried out in 5.0 mM Fe $[(CN)_6]^{3-/4-}$ and 0.1 M KNO_3 as shown in Fig. 2. Compared with bare GCE (curve a), the current response increased when porous graphene modified on GCE surface (curve c), and the peak difference between anodic and cathodic peaks (ΔEp) at PGN/GCE is smaller, indicating that the porous graphene is an excellent electric conducting material. Whereas, the current response of AgNPs-GN modified electrode decreased in curve b. The reason, we think, may be ascribed to the quantum size effect of nanoparticles. According to Kubo theory (Chen et al., 2010), the smaller of silver nanoparticle, the more obvious of quantum size effect, and the poor conductivity it has.

Electrochemical impedance spectroscopy (EIS) is also an effective method for monitoring the interfacial properties of surface-modified electrodes (Liao et al., 2010). In the Nyquist plots of the impedance spectra, a semicircle portion observed at higher frequencies would correspond to the charge-transfer limited process, and a linear section at the lower frequencies is attributed to the diffusion-limited process. The semicircle diameter corresponds to the electron-transfer resistance (Ret), which can be used to describe the interface properties of the electrode. Fig. 2B shows the Nyquist plots of different electrodes using $Fe[(CN)_6]^{3-/4-}$ as the electrochemical probe, and the inset is the fits of equivalent circuit. It is observed that the bare GC electrode after polishing shows a semicircle domain about 65 Ω at high frequencies and a linear part at low frequencies (curve a). When the GC electrode is modified with AgNPs/GN, the Ret increases to 75 Ω (curve b). Most importantly, the Ret of PGN/GCE (curve c) significantly decreases, implying the favorable conductivity of porous graphene. This result indicates that the higher electron conduction pathways are formed on the porous graphene between the electrode and electrolyte. This is agreed with the results from cyclic voltammetry (Fig. 2A).

In addition, a comparative study was carried out by calculating the electroactive surface areas of the three kinds of electrodes: bare GCE, GN/GCE and PGN/GCE. From Fig. S1 in the Supporting information, the electroactive surface areas of electrodes were calculated in the trend of bare GCE (0.0504 cm^2) < GN/GCE (0.0836 cm^2) < PGN/GCE (0.1470 cm^2), suggesting that PGN could

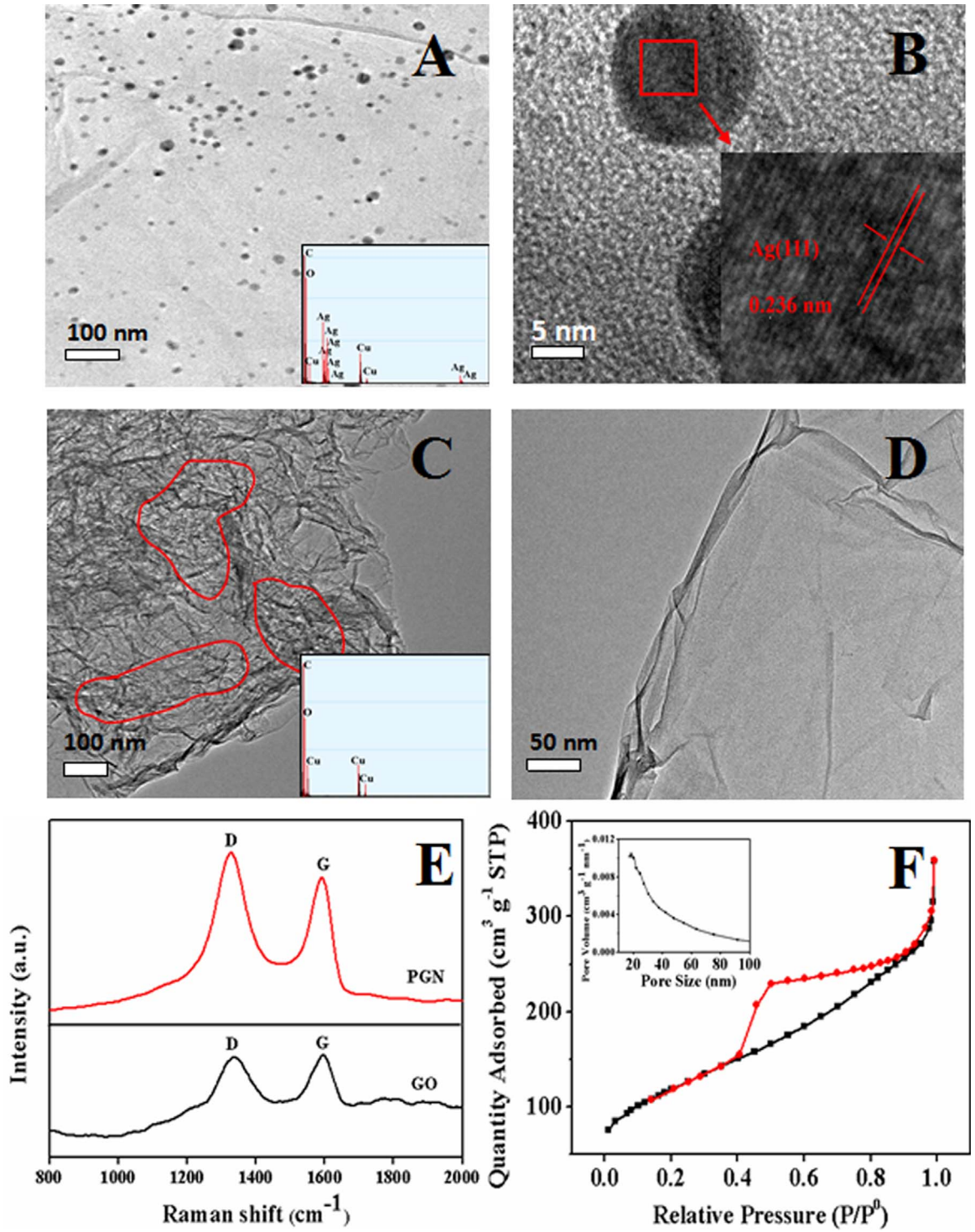

Fig. 1. TEM images of AgNPs-GN (A), PGN (C) and GN (D); Insets are EDX images of AgNPs-GN (up) and PGN (down); HRTEM image of AgNPs-GN (B); Raman spectra of PGN and GO (E); Nitrogen adsorption/desorption isotherm and pore size distribution (inset) of PGN (F).

enlarge the specific surface area because of its porous structure.

3.2. Direct electrochemistry of HRP/PGN/GCE-1

As stated in the introduction section, the porous graphene carbon nanomaterial could serve as excellent support matrix for immobilizing enzyme on the electrode surface. Thus direct electrochemistry of HRP enzyme is studied as shown in Fig. S2. The results suggested that the porous graphene could immobilize enzyme effectively, and provide a favorable microenvironment to retain the bioactivity of HRP.

3.3. Electrochemical response of H_2O_2 at HRP/PGN/GCE-2

Fig. 3 shows the cyclic voltammograms at HRP/PGN/GCE-2 in 1.0 mM H_2O_2 and N_2-saturated 0.2 M PBS. As a comparison, HRP/GCE-2, PGN/GCE-2 and HRP/GN/GCE-2 were also prepared under the same conditions to detect H_2O_2. For HRP/GCE-2 (curve a), a poor cathodic peak current at around −0.6 V was observed, suggesting that the reduction of H_2O_2 was hardly achieved due to

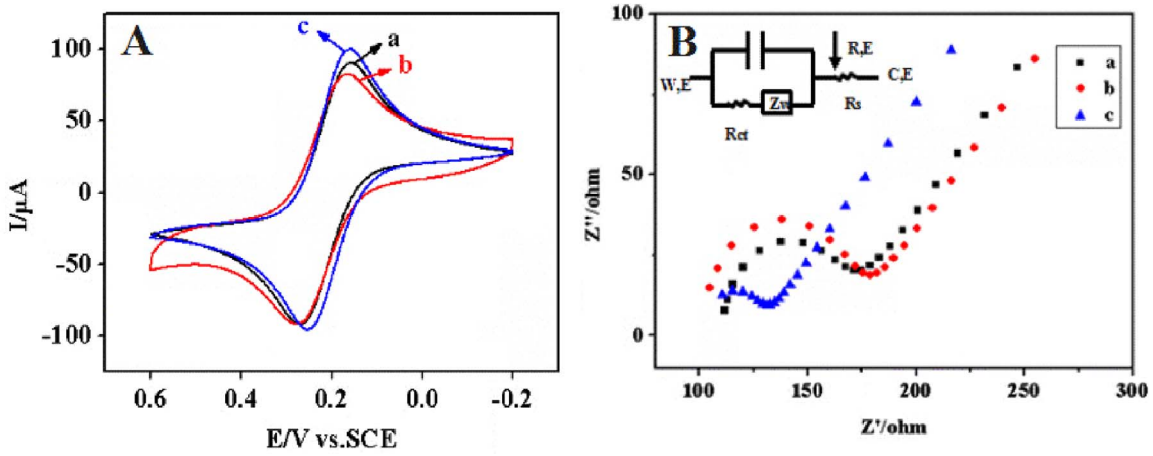

Fig. 2. The CV (A) and EIS (B) of (a) bare GCE, (b) AgNPs-GN/GCE, (c) PGN/GCE in 5.0 mM $Fe[(CN)_6]^{3-/4-}$ and 0.1 M KNO_3.

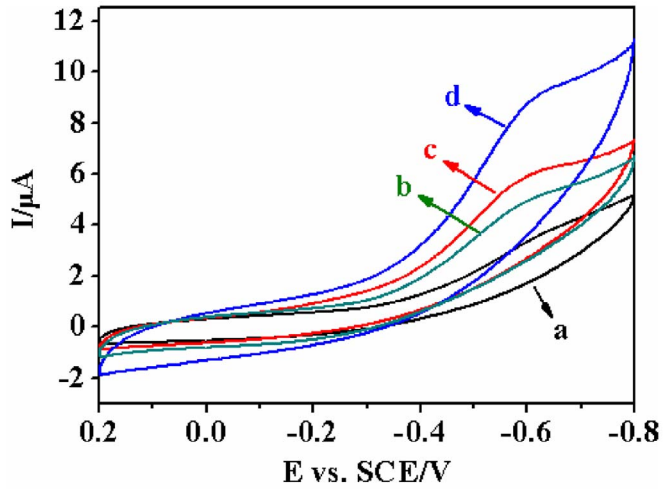

Fig. 3. Cyclic voltammograms of different electrodes in 1.0 mM H_2O_2 and N_2-saturated 0.2 M PBS (pH 7.0): (a) HRP/GCE-2 (b) HRP/GN/GCE-2 (c) PGN/GCE-2 (d) HRP/PGN/GCE-2 at 50 mV/s.

slow electrode kinetics and high overpotential (Chen et al., 2012). Generally, the enzyme is easy to lose its bioactivity when directly adsorbed on a bare electrode surface (Hong et al., 2006). As PGN was modified on the electrode (curve c), the peak current increased, because the porous structure of PGN could provide large active area to contact H_2O_2 and facilitate its electron transfer. Most important, we found that the current enhanced obviously as shown in curve d when the electrode modified by HRP@PGN. It was 3.2 times and 1.5 times as large as that of HRP/GCE-2 (curve a) and PGN/GCE-2 (curve c), respectively. The excellent current respond may result from the following two factors. On the one hand, PGN could load on great amount of HRP and offer a biocompatible microenvironment for retaining the HRP bioactivity. On the other hand, the nanoporous structure of PGN may confine H_2O_2 in the pores to obtain a higher occurrence of H_2O_2-active site encounters and then a higher activity. The result of comparing curve b and d further illustrates that HRP@PGN shows excellent electrocatalytic effect toward H_2O_2.

3.4. Performance of the hydrogen peroxide sensor

3.4.1. Optimization of the experimental variables

In order to obtain an efficient sensor for detection H_2O_2, the analytical conditions, such as the concentration ratio of HRP and PGN, the deposition volume of HRP@PGN, were optimized by the prepared hydrogen peroxide sensor as shown in Fig. S3. The experiment results show that HRP/PGN/GCE-2 has the best response current for H_2O_2 at 5:1 of concentration ratio for HRP and PGN. Our observations also indicate that the sensitivity response increased with the increasing volume of deposition and reached a summit at a volume of 6 μL of HRP@PGN, afterward it decreased upon addition of much larger deposition volume. Therefore, 5:1 of concentration ratio for HRP and PGN and 6 μL of HRP@PGN were used in the experiment.

3.4.2. Amperometric response and calibration curve

The chronoamperometry is a control potential step of electrochemical analysis method. Under the optimal experimental conditions, the amperometric responses of the HRP/PGN/GCE-2 are shown in Fig. 4 by successive additions of H_2O_2 to N_2-saturated 0.2 M PBS (pH 7.0) at an applied potential of −0.7 V. The current responses of the sensor increased along with H_2O_2 concentrations and the relevant linear range for the detection of H_2O_2 contained two segments: the response to logarithm of the H_2O_2 concentration showed linear range from 8.0×10^{-11} to 6.64×10^{-7} mol/L, and the linear regression equation was $Ip(\mu A) = 0.1615 lg[H_2O_2] + 5.6702$ with a correlation coefficient of 0.9952 (Fig. 4B). Another linear relationship could be established between the peak current and the concentration of H_2O_2 in the range from 2.77×10^{-6} to 8.35×10^{-4} mol/L, and the linear regression equation was $Ip(\mu A) = 0.0052[H_2O_2](\mu M) + 4.7364$ with a correlation coefficient of 0.9987 (Fig. 4D). Moreover, the obtained biosensor also shows very low detection limit (ratio of signal-to-noise S/N=3) of 2.67×10^{-11} mol/L. A comparison of linear range and detection limit for HRP/PGN/GCE-2 with other H_2O_2 sensors reported in literature are summarized in Table S1. The data demonstrate the analytical parameters of HRP/PGN/GCE-2 are better than those obtained at several electrodes reported recently, which is ascribed to the 3D architectures of porous grapheme. Moreover, the outstanding merit of the enzymatic H_2O_2 sensor lies in its super low detection limit, excellent selectivity and sensitivity.

3.4.3. Interference immunity, reproducibility and stability of the H_2O_2 sensor

Since there are a variety of interferences coexisting in biological samples, the sensor used for the practical measurements should have significant specificity against potential interferences. Ascorbic acid (AA), Dopamine (DA) and uric acid (UA) are three of the most commonly existing interference species in the physiological environment. Fig. 5A showed the current responses of the sensor

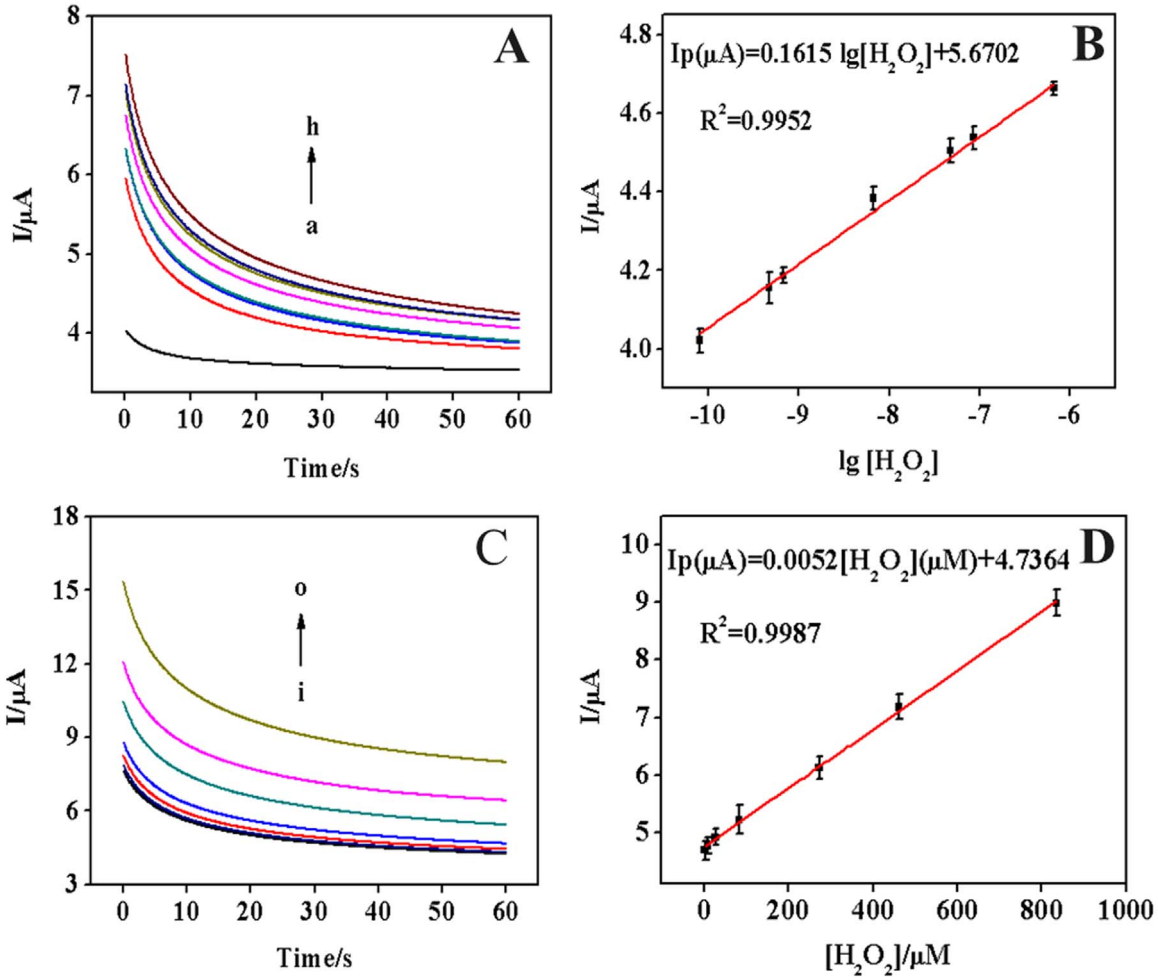

Fig. 4. (A) The chronoamperometry current–time curve of HRP/PGN/GCE-2 in N_2-saturated 0.2 M PBS (pH 7.0) containing various concentrations of H_2O_2 (from a to h: 0, 8.0×10^{-11}, 4.74×10^{-10}, 6.71×10^{-10}, 6.73×10^{-9}, 4.75×10^{-8}, 8.61×10^{-8}, 6.64×10^{-7} M), at -0.7 V; (B) the calibration curve between current and lg[H_2O_2]. (C) The chronoamperometry current–time curve of HRP/PGN/GCE-2 with successive addition of H_2O_2 (from i to o: 2.77×10^{-6}, 8.48×10^{-6}, 2.75×10^{-5}, 8.42×10^{-5}, 2.73×10^{-4}, 4.61×10^{-4}, 8.35×10^{-4} M) to N_2-saturated 0.2 M PBS (pH 7.0) at -0.7 V; (D) the calibration plots illustrating the linear electrode response to H_2O_2 addition.

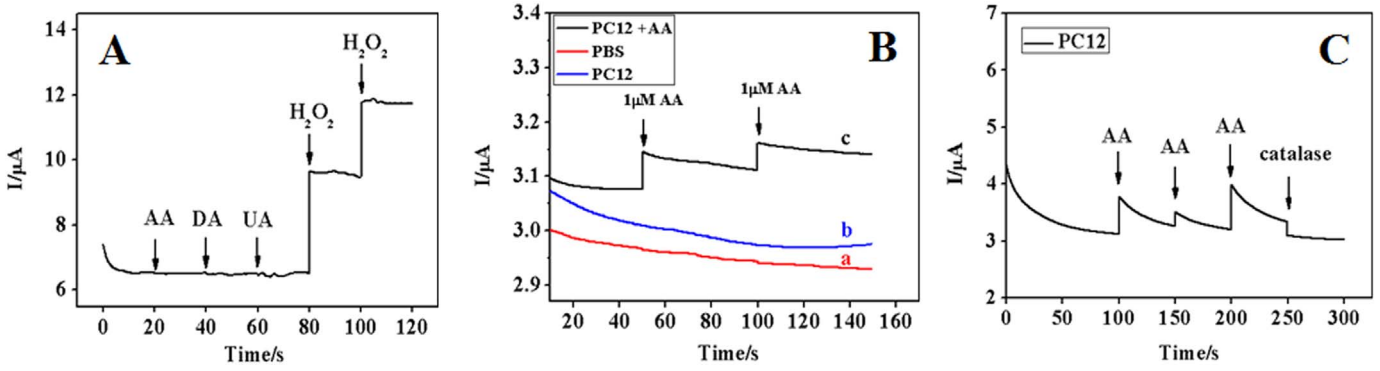

Fig. 5. (A) Amperometric i-t response of HRP/PGN/GCE-2 upon the successive addition of AA (0.2 mM), DA (0.2 mM), UA (0.2 mM), and H_2O_2 (0.2 mM) into 0.2 M PBS(pH 7.0) with an applied potential -0.7 V under a stirring condition; (B) time course of the blank PBS (a); the PC12 cells (b); the H_2O_2 release from PC12 cells upon the successive addition of 1 μM AA (c); (C) amperometric responses obtained at the HRP/PGN/GCE-2 in the presence of PC12 cells at -0.7 V with the successive addition of 1 μM AA and 300 units/mL catalase.

with the addition of 0.2 mM AA, 0.2 mM DA, 0.2 mM UA, 0.2 mM H_2O_2 and a second injection of 0.2 mM H_2O_2 in the same sample. There were remarkable current responses with the addition of 0.2 mM H_2O_2, while AA, DA, and UA yielded little current response at the HRP/PGN/GCE-2 under the applied negative potential, verifying that the HRP/PGN/GCE-2 could be used for the selective and sensitive detection of H_2O_2.

The reproducibility of the modified electrode was also tested. Five independently HRP/PGN/GCE-2 were estimated from the response to 1.0 mM H_2O_2, and showed a good reproducibility with an acceptable RSD of 3.23% for the sensitivity to H_2O_2 in Fig. S4A. Moreover, it could retain 85.14% of the original value after 50 consecutive measurements as shown in Fig. S4B.

3.5. Detection of H_2O_2 release from living cells

H_2O_2 is one of the most important molecules related to many cell functions, and is a potential marker for tumor cells (Sun et al., 2012). Owing to the remarkable analytical advantages of the developed sensor, in this work, HRP/PGN/GCE-2 was also utilized for the real-time detection of H_2O_2 released from living cells. Here, rat adrenal medulla pheochromocytoma cell (PC12) was chosen as the model cancer cell, and ascorbic acid (AA) was employed as the stimulant agent to induce H_2O_2 generation from cancer cells. Fig. 5B depicts the amperometric responses obtained at the HRP/PGN/GCE-2 under an applied potential of −0.7 V versus SCE in different conditions. Curve b describes the response of modified electrode in PC12 cells, and one can see that the current is higher than that in blank PBS (curve a), illustrating HRP/PGN/GCE-2 is able to detect the ROS generation from cancer cells. More importantly, the current response of curve b will increase slowly when the time is over 120 s, revealing further the PC12 cells could release ROS constantly by themselves and can be detected sensitively by the constructed electrode. When PC12 cells were stimulated by AA, as shown in curve c, the current responses increased significantly accompanying by the successive addition of AA in a few seconds. In order to confirm whether the increased current signal is caused by the H_2O_2 produced from the stimulated cells, we carried out another experiment by adding the catalase, which is a selective scavenger of H_2O_2 (Wang et al., 2013). As shown in Fig. 5C, the increased currents were also observed in the living cells by successive addition of AA. However, as injecting the catalase at 250 s, the current response decreased immediately to its background level due to the decomposition of H_2O_2. These results together suggested that the amperometric responses are ascribed to the electrochemical reduction of H_2O_2 released by living cells upon being stimulated by AA, which are consistent with the earlier reports (Maji et al., 2014; Zhang et al., 2014b). Moreover, Fig. S5 shows the bright-field microscope images of PC12 cells in different conditions, indicating the good biocompatibility of HRP/PGN/GCE-2. Thus, we can draw the conclusions that HRP/PGN/GCE-2 has the super sensitive electrochemical response and could be effectively used for reliable and durable determination of H_2O_2 in living cells.

4. Conclusions

In summary, we have synthesized a new type of supporting material for immobilizing enzyme, and explored its practical application as an electrode material in an electrochemical sensor for in situ detecting the H_2O_2 release from living cells. These 3D architectures of porous graphene exhibit high specific surface area as well as fast mass and electron transport kinetics due to the combination of porous structures and the excellent intrinsic properties of graphene. These advantages make PGN nanocomposites a promising candidate for electrochemical sensors and biosensors design. More importantly, the electrochemical sensor fabricated from the HRP@PGN has shown great potential application for H_2O_2 detection in biological environments. Since H_2O_2 is a byproduct of many oxidative biological reactions, which is very significant in biochemical, physiological, and pathological investigation, this work serves as a pathway for the application of HRP/PGN/GCE in the fields of electrochemical sensing and bioanalysis.

Note

The authors declare no competing financial interest.

Acknowledgments

This work was supported by the National Natural Science Foundation of China (Nos. 21565021, 21265018, and 21563027), and Program for Chang Jiang Scholars and Innovative Research Team, Ministry of Education, China (Grant no. IRT1283).

Appendix A. Supplementary information

Supplementary data associated with this article can be found in the online version at http://dx.doi.org/%2010.1016/j.bios.2016.08.015.

References

Cao, H., Zhou, X., Zheng, C., Liu, Z., 2015. Carbon 89, 41–46.
Chang, H., Wang, X., Shiu, K.K., Zhu, Y., Wang, J., Li, Q., Chen, B., Jiang, H., 2013. Biosens. Bioelectron. 41, 789–794.
Chen, C., Hong, X., Xu, T., Chen, A., Lu, L., Gao, Y., 2016. Synth. Met. 212, 123–130.
Chen, J., Liu, J., Sun, X., Chen, Y., 2010. Introduction to Nanomaterials Science. Higher Education Press, Beijing, p. 114.
Chen, W., Cai, S., Ren, Q.Q., Wen, W., Zhao, Y.D., 2012. Analyst 137 (1), 49–58.
Fan, Z., Zhao, Q., Li, T., Yan, J., Ren, Y., Feng, J., Wei, T., 2012. Carbon 50 (4), 1699–1703.
Feyzizarnagh, H., Park, B.-W., Sharma, L., Patania, M.M., Yoon, D.Y., Kim, D.-S., 2016. Sens. Bio-Sens. Res. 7, 38–41.
Fu, X., Shen, W., Yao, T., Hou, W., 2006. Physical Chemistry, Fifth Ed. Higher Education Press, Beijing, pp. 359–392.
Han, S., Wu, D., Li, S., Zhang, F., Feng, X., 2014. Adv. Mater. 26 (6), 849–864.
Hong, J., Ghourchian, H., Moosavi–Movahedi, A.A., 2006. Electrochem. Commun. 8 (10), 1572–1576.
Jiang, L., Fan, Z., 2014. Nanoscale 6 (4), 1922–1945.
Li, D., Muller, M.B., Gilje, S., Kaner, R.B., Wallace, G.G., 2008. Nat. Nanotechnol. 3 (2), 101–105.
Liao, Y., Yuan, R., Chai, Y., Zhuo, Y., Yang, X., 2010. Anal. Biochem. 402 (1), 47–53.
Lippert, A.R., Van de Bittner, G.C., Chang, C.J., 2011. Acc. Chem. Res. 44 (9), 793–804.
Liu, J., Bo, X., Zhao, Z., Guo, L., 2015a. Biosens. Bioelectron. 74, 71–77.
Liu, Y., Liu, X., Li, M., Liu, Y., Guo, Z., Xue, Z., Lu, X., 2015b. RSC Adv. 5 (121), 100268–100271.
Maji, S.K., Sreejith, S., Mandal, A.K., Ma, X., Zhao, Y., 2014. ACS Appl. Mater. Interfaces 6 (16), 13648–13656.
Oh, W.-K., Jeong, Y.S., Kim, S., Jang, J., 2012. ACS Nano 6 (10), 8516–8524.
Pagliari, F., Mandoli, C., Forte, G., Magnani, E., Pagliari, S., Nardone, G., Licoccia, S., Minieri, M., Di Nardo, P., Traversa, E., 2012. ACS Nano 6 (5), 3767–3775.
Qin, X., Luo, Y., Lu, W., Chang, G., Asiri, A.M., Al-Youbi, A.O., Sun, X., 2012. Electrochim. Acta 79, 46–51.
Rhee, S.G., Chang, T.S., Jeong, W., Kang, D., 2010. Mol. Cells 29 (6), 539–549.
Sint, K., Wang, B., Král, P., 2008. J. Am. Chem. Soc. 130 (49), 16448–16449.
Sun, X., Guo, S., Liu, Y., Sun, S., 2012. Nano Lett. 12 (9), 4859–4863..
Trachootham, D., Alexandre, J., Huang, P., 2009. Nat. Rev. Drug Discov. 8 (7), 579–591.
Wang, T., Zhu, H., Zhuo, J., Zhu, Z., Papakonstantinou, P., Lubarsky, G., Lin, J., Li, M., 2013. Anal. Chem. 85 (21), 10289–10295.
Wu, P., Cai, Z., Gao, Y., Zhang, H., Cai, C., 2011. Chem. Commun. 47 (40), 11327–11329.
Xi, J., Zhang, Y., Wang, N., Wang, L., Zhang, Z., Xiao, F., Wang, S., 2015. ACS Appl. Mater. Interfaces 7 (9), 5583–5590.
Xi, Q., Chen, X., Evans, D.G., Yang, W., 2012. Langmuir 28 (25), 9885–9892.
Xu, J., Li, Q., Yue, Y., Guo, Y., Shao, S., 2014. Biosens. Bioelectron. 56, 58–63.
Yuan, L., Lin, W., Xie, Y., Chen, B., Zhu, S., 2012. J. Am. Chem. Soc. 134 (2), 1305–1315.
Zhang, L.N., Deng, H.H., Lin, F.L., Xu, X.W., Weng, S.H., Liu, A.L., Lin, X.H., Xia, X.H., Chen, W., 2014a. Anal. Chem. 86 (5), 2711–2718.
Zhang, Y., Bai, X., Wang, X., Shiu, K.K., Zhu, Y., Jiang, H., 2014b. Anal. Chem. 86 (19), 9459–9465.
Zhang, Y., Wu, C., Zhou, X., Wu, X., Yang, Y., Wu, H., Guo, S., Zhang, J., 2013. Nanoscale 5 (5), 1816–1819.
Zhou, D., Cui, Y., Xiao, P.W., Jiang, M.Y., Han, B.H., 2014. Nat. Commun. 5, 4716.